Synthesis and Ultrasonic Investigation of Graphene Oxide and Reduced Graphene Oxide Nanosuspension with Ethylene Glycol

Kenya Kandwal [1] 🆔 , **Alok Jain** [1,*]

[1] Department of Physics, School of Chemical Engineering and Physical Sciences, Lovely Professional University, Jalandhar-144411 Punjab, India
* Correspondence: alok.jain@lpu.co.in;

Abstract: The Original Hummer's Method was used to produce Graphene Oxide. Hydrazine monohydrate was used to produce Reduced Graphene Oxide by the Graphene Oxide sample. The processed Reduced Graphene Oxide was confirmed by numerous characterization methodologies: RAMAN, X-ray diffraction, Field emission scanning electron microscopy, Energy-dispersive X-ray spectroscopy, and Fourier transform infrared. The numerous characterization methodologies verified the manufacture of Graphene Oxide and the transformation of Reduced Graphene Oxide from Graphene Oxide. The ultrasonication process of double distilled water was used for 24 hours to produce reduced graphene oxide nanosuspension. Further existence of reduced graphene oxide was confirmed by the ultraviolet-visible spectroscopy operating procedure in the nanosuspension. The dimension of reduced graphene oxide fragments was verified by an Ethylene Glycol solution's dynamic light scattering technique. Viscosity, density, and ultrasonic velocity for every concentration were calculated. Other parameters, such as acoustical impedance, intermolecular length, and adiabatic compressibility, are also calculated from investigated data.

Keywords: viscosity; bulk modulus; temperature; adiabatic compressibility; acoustical impedance; nanosuspension; graphene.

1. Introduction

Colloidal dispersion leads to the formation of nanosuspension nanoparticles ranging between 100-500 nm [1]. Carbon nanotubes, carbide metals, and oxides were used as basic-components for the nanoparticles. Nanosized particles could be essential for more deficient heat transfer utilization as these nanostructures have high thermal conductance [2] and enormous surface area [9] [3] that can be deployed in various industries such as electronics. The literature discusses how the nanoparticles' greater surface area accounts for the majority of their remarkable characteristics. The fluid we are mixing has better overall qualities when we add nanoparticles with a bigger surface area. The nanoparticles may interact with the solvent molecules because of their very tiny size. Heat causes the liquid's molecules to move in an erratic zigzag pattern. Molecules clash with the suspension's nanoparticle as a result of this motion. Nanosuspension characteristics are further advanced by a selection of nanofluids [4]. Therefore, nanosuspension research aims to attempt to produce steady nanosuspension for commercial operation [5]. Utilizing ultrasound is the proven methodology for synthesizing

fluid nanosuspension by dispersed trapped nanoparticles. The research has shown enhancements in nanosuspension stability with an extension of the sonication period. The nanosuspension's ability to stay steady depends on the selection of nanoparticles and the period of sonication. Thus, developing steady nanosuspension that can be utilized for industrial purposes is the primary concern. Researchers are studying the density, viscosity, and ultrasonic velocity of nanosuspensions. Given that the nanoparticles' surface volume % is quite high, the thermoacoustic characteristics of the nanosuspension may be greatly enhanced.

Regarding the chemical and physical characteristics of the process steps, graphene has been among the most relevant findings in the past ten years. Since its development, it has exhibited a wide range of characteristics, including the strongest material, high thermal conductivity, high electron mobility, and high electron density [6]. This material encounters two significant obstacles: fabricating stable suspension and industrial-scale productivity [7]. Graphene was one of the key materials we found and investigated in the last ten years. Numerous studies have considered and reported several features since its discovery in 2004 collectives. First off, a lot of studies have been done on the graphene production process itself. Several teams are trying to figure out a sustainable and eco-friendly method of producing graphene. Although graphene presents numerous opportunities for research and development, there are still certain gaps in the field. For example, it is impossible to produce graphene at an industrial scale, and the process of creating it involves toxic gases. Graphene can only be suspended in a very small number of solvents.

In this study, we synthesized an ethylene glycol-based rGO (reduced graphene oxide) nanosuspension with concentration ranges. Studies on the interaction between fluid, morphology, and structures have been performed and examined [8]. rGO-Ethylene Glycol nanosuspension intermolecular interaction was seen at numerous temperatures and concentrations ranging between 298K and 314K. Acoustic, adiabatic compressibility, ultrasound, mean free path, and impedance were examined [9,10].

2. Material and Methods

From Sigma Aldrich, sodium nitrate and hydrazine monohydrates have been purchased. Ethylene Glycol (EG), H_2SO_4, HCL, $KMnO_4$, and ammonia were purchased from CDH. H_2O_2 was purchased from Fisher Scientific. All components were AR grade. Triple distilled water was used throughout the experiment.

5 g of Sodium Nitrate and 5 g of graphite powder were combined with sulfuric acid of 250 ml in a 1000 ml beaker. To ensure the temperature ranges between 0°C-10°C, an ice bath has been built around the beaker. The suspension was stirred for over 3 Hours at his temperature. At a range of temperature less than 10°C, 15 grams of potassium permanganate was slowly added and held at a temperature of 35°C till it turned brown.100 ml of water was slowly introduced to the mixture, ensuring a temperature of less than 90°C. 500 ml of water was additionally added while being continuously stirred. To terminate the reaction, 50 ml of hydrogen peroxide was added to the reaction. With deionized water and 10% HCl solution was continuously washed. The GO powder was extracted after the filtering solution was vacuum-dried.

The synthesized graphene oxide GO powder is split into two equal proportions to synthesize rGO from GO. A homogenous concentration of GO powder in ionized powder(2 mg/ml) was obtained by employing the ultrasonication technique. A few drops of ammonia

were introduced to the solution to stabilize the PH ranging between 9 and 10. Hydrazine monohydrate (1 µl for 3 mg of GO) was introduced to the solution. It was stirred for 4 hours at 95°C, which produced the black precipitate. Black rGO precipitate was rinsed, vacuum-dried, and filtered after it reached room temperature. The ultrasonication was employed to synthesize nanosuspension in the following suspensions- 0.8 mg/ml, 0.4 mg/ml, 0.2 mg/ml, 0 mg/ml, 0.6 mg/ml, and 1 mg/ml.

3. Results and Discussion

X-ray diffraction (XRD) in the range of 2Ө=20°-70° was analyzed using (Panalytical X'Pret Pro) X-ray diffraction with Cu Kα radiation(k=1.5406) at a voltage of 40 KV and with a current of 40 mA. Shimadzu 8400 spectrometer was employed for FTIR Spectro (KBr pellets). Micro-level imaging of the sample was acquired by Nova Nano FESEM 450 with connected EDAX. Confocal Raman Spectrometer Airix-STR 500 was employed to analyze Raman spectra running between 800-2000 cm^{-1} at room temperature. Shimadzu UV-1800 Spectrometer was employed to analyze UV-VS spectra. Malvern- Zetasizer Nano ZS90 was employed to confirm the average particle size. Mittal Interferometer M-81 determined the ultrasonic velocity of the synthesized sample with a 2MHz fixed frequency. A pycnometer was employed to measure the density. The LMDV-200 Layman model evaluated the viscosity of the synthesized sample.

Table 1. GO-EG nanosuspension.

Concentration (mg/ml)	Temperature (K)	Jacobson Coefficient (K_T)	Average Velocity (m/s)	Density (Kg/m³)	Viscosity (Pa-s)	Adiabatic Compressibility(β) =1/{(density*velocity²} (1/Pa)
0	299	2.056	1670.77	1121.1	0.012193	3.20E-10
0.2	299	2.056	1670.07	1120.9	0.016103	3.20E-10
0.4	299	2.056	1669.09	1120.7	0.01363	3.20E-10
0.6	299	2.056	1665.33	1120.2	0.012383	3.22E-10
0.8	299	2.056	1663.54	1119.8	0.012126	3.23E-10
1	299	2.056	1661.08	1119.4	0.010806	3.24E-10
0	304	2.075	1653.08	1118.4	0.01103	3.27E-10
0.2	304	2.075	1652.23	1117.8	0.014249	3.28E-10
0.4	304	2.075	1651.15	1117.3	0.012378	3.28E-10
0.6	304	2.075	1649.15	1116.8	0.011573	3.29E-10
0.8	304	2.075	1645.23	1116.3	0.010988	3.31E-10
1	304	2.075	1636.92	1116	0.0102	3.34E-10
0	309	2.094	1633.85	1115.4	0.01036	3.36E-10
0.2	309	2.094	1631.23	1114.7	0.012795	3.37E-10
0.4	309	2.094	1628.69	1114.1	0.011148	3.38E-10
0.6	309	2.094	1625.54	1114.1	0.010336	3.40E-10
0.8	309	2.094	1622.92	1113.8	0.010171	3.41E-10
1	309	2.094	1621.54	1113.4	0.009789	3.42E-10
0	314	2.11	1618.46	1113.6	0.00944	3.43E-10
0.2	314	2.11	1615.08	1113.1	0.010765	3.44E-10
0.4	314	2.11	1613.46	1112.3	0.010288	3.45E-10
0.6	314	2.11	1612.15	1112	0.009604	3.46E-10
0.8	314	2.11	1608.62	1111	0.009346	3.48E-10
1	314	2.11	1605.38	1110.5	0.009213	3.49E-10

Table 2. GO-EG nanosuspension.

Concentration (mg/ml)	Temperature (K)	Acoustic impedance Z = Density * Velocity (Z)	Attenuation (α/f^2) (m^{-1})	Bulk Modulus K = $Velocity^2$ * Density (Pa)	Relaxation Time $\tau = 4\beta\eta/3$ (s)	Intermolecular Free Length Lf = Jacobson Constant * Adiabatic $Compressibility^{1/2}$ (m)
0	299	1873099.385	6.13119E-14	3129516818	5.19E-12	3.28E-10
0.2	299	1871980.601	8.1087E-14	3126337202	6.87E-12	3.29E-10
0.4	299	1870550.182	6.87693E-14	3122118303	5.82E-12	3.29E-10
0.6	299	1865506.4	6.2927E-14	3106689991	5.31E-12	3.31E-10
0.8	299	1862830.369	6.18466E-14	3098889967	5.22E-12	3.32E-10
1	299	1859409.508	5.53759E-14	3088622224	4.66E-12	3.33E-10
0	304	1848801.231	5.7402E-14	3056210650	4.81E-12	3.39E-10
0.2	304	1846863.554	7.43068E-14	3051444790	6.23E-12	3.40E-10
0.4	304	1844834.192	6.47036E-14	3046105072	5.42E-12	3.41E-10
0.6	304	1841775.015	6.0743E-14	3037370350	5.08E-12	3.42E-10
0.8	304	1836571.108	5.8112E-14	3021583296	4.85E-12	3.43E-10
1	304	1826806.154	5.47872E-14	2990341150	4.55E-12	3.47E-10
0	309	1822392	5.59917E-14	2977508160	4.64E-12	3.52E-10
0.2	309	1818332.081	6.95288E-14	2966117840	5.75E-12	3.53E-10
0.4	309	1814526.1	6.08926E-14	2955304701	5.03E-12	3.54E-10
0.6	309	1811012.4	5.67904E-14	2943870311	4.68E-12	3.56E-10
0.8	309	1807611.723	5.61696E-14	2933614779	4.62E-12	3.57E-10
1	309	1805420.923	5.42161E-14	2927559466	4.46E-12	3.58E-10
0	314	1802318.769	5.25731E-14	2916983608	4.31E-12	3.62E-10
0.2	314	1797742.123	6.03571E-14	2903491817	4.94E-12	3.63E-10
0.4	314	1794653.269	5.78949E-14	2895604025	4.74E-12	3.64E-10
0.6	314	1792715.077	5.41932E-14	2890132506	4.43E-12	3.65E-10
0.8	314	1787171.692	5.31367E-14	2874871879	4.33E-12	3.67E-10
1	314	1782779.615	5.27197E-14	2862046967	4.29E-12	3.69E-10

Table 3. rGO-EG nanosuspension.

Concentration (mg/ml)	Temperature (K)	Jacobson Coefficient (K_T)	Average Velocity (m/s)	Density (Kg/m^3)	Viscosity (Pa-s)	Adiabatic Compressibility(β) =1/{(density*velocit y^2} (1/Pa)
0	299	2.056	1665.77	1121.1	0.012193	3.21E-10
0.2	299	2.056	1663.38	1120.2	0.01397	3.23E-10
0.4	299	2.056	1659.46	1119.7	0.013781	3.24E-10
0.6	299	2.056	1655.38	1119.5	0.013685	3.26E-10
0.8	299	2.056	1653.38	1119.2	0.01298	3.27E-10
1	299	2.056	1650.38	1118.7	0.012516	3.28E-10
0	304	2.075	1653.08	1118.4	0.01103	3.27E-10
0.2	304	2.075	1651.85	1117.7	0.012539	3.28E-10
0.4	304	2.075	1648.85	1117.1	0.012243	3.29E-10
0.6	304	2.075	1645.92	1116.3	0.011473	3.31E-10
0.8	304	2.075	1642.92	1115.8	0.011168	3.32E-10
1	304	2.075	1640.00	1115.2	0.010779	3.33E-10
0	309	2.094	1638.85	1115.4	0.01036	3.34E-10
0.2	309	2.094	1635.77	1114.7	0.011225	3.35E-10
0.4	309	2.094	1632.69	1113.9	0.011041	3.37E-10
0.6	309	2.094	1629.77	1113.4	0.01025	3.38E-10
0.8	309	2.094	1626.85	1112.8	0.009879	3.40E-10
1	309	2.094	1623.85	1111.8	0.0095	3.41E-10
0	314	2.11	1618.46	1113.6	0.00944	3.43E-10
0.2	314	2.11	1615.38	1112.3	0.009728	3.45E-10
0.4	314	2.11	1612.31	1111.7	0.009518	3.46E-10
0.6	314	2.11	1609.46	1111.1	0.008904	3.47E-10
0.8	314	2.11	1605.46	1110.4	0.008421	3.49E-10
1	314	2.11	1602.46	1109.4	0.008134	3.51E-10

Table 4. rGO-EG nanosuspension.

Concentration (mg/ml)	Temperature (K)	Acoustical impedance Z = Density * Velocity (Z)	Attenuation (α/f^2) (m^{-1})	Bulk Modulus K = $Velocity^2$ * Density (Pa)	Relaxation Time $\tau = 4\beta\eta/3$ (s)	Intermolecular Free Length Lf = jacobson Constant * Adiabatic $Compressibility^{1/2}$ (m)
0	299	1867493.885	6.18657E-14	3110813852	5.23E-12	3.30E-10
0.2	299	1863323.446	7.12444E-14	3099423554	6.01E-12	3.32E-10
0.4	299	1858099.085	7.08131E-14	3083443966	5.96E-12	3.33E-10
0.6	299	1853203.077	7.0852E-14	3067763863	5.95E-12	3.35E-10
0.8	299	1850468.062	6.74642E-14	3059535424	5.66E-12	3.36E-10
1	299	1846285.269	6.54385E-14	3047080804	5.48E-12	3.37E-10
0	304	1848801.231	5.7402E-14	3056210650	4.81E-12	3.39E-10
0.2	304	1846268.446	6.54407E-14	3049751432	5.48E-12	3.40E-10
0.4	304	1841926.038	6.42785E-14	3037052664	5.37E-12	3.42E-10
0.6	304	1837343.931	6.0605E-14	3024126776	5.06E-12	3.43E-10
0.8	304	1833173.569	5.93398E-14	3011763161	4.94E-12	3.44E-10
1	304	1828928	5.76119E-14	2999441920	4.79E-12	3.46E-10
0	309	1827969	5.54808E-14	2995759965	4.61E-12	3.49E-10
0.2	309	1823391.962	6.04909E-14	2982648466	5.02E-12	3.51E-10
0.4	309	1818655.962	5.988E-14	2969305599	4.96E-12	3.53E-10
0.6	309	1814585.062	5.59142E-14	2957354900	4.62E-12	3.54E-10
0.8	309	1810354.4	5.421E-14	2945168093	4.47E-12	3.55E-10
1	309	1805392.154	5.24675E-14	2931679105	4.32E-12	3.57E-10
0	314	1802318.769	5.25731E-14	2916983608	4.31E-12	3.62E-10
0.2	314	1796792.308	5.45481E-14	2902510651	4.47E-12	3.63E-10
0.4	314	1792402.462	5.37056E-14	2889904276	4.39E-12	3.65E-10
0.6	314	1788272.715	5.05405E-14	2878156156	4.13E-12	3.67E-10
0.8	314	1782704.492	4.81865E-14	2862063497	3.92E-12	3.69E-10
1	314	1777770.831	4.68495E-14	2848809381	3.81E-12	3.70E-10

3.1. Analyzing and elements.

The structural characterization of GO and rGO samples is analyzed using Field emission scanning electron microscopy SEM [11]. High-magnification SEM pictures 1(a) and 1(b) for GO and rGO, respectively, allowed for observing the general morphology of the various layers. The folded and wrinkled graphene sheets are visible in Figure 1 thanks to SEM photos.
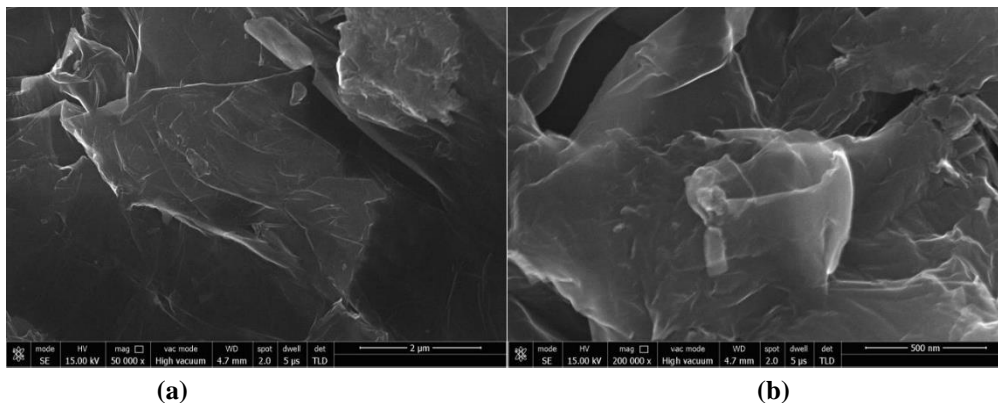

(a)   **(b)**

Figure 1. (a) FESEM image of GO; **(b)** FESEM image of rGO.

Additionally, the Energy-dispersive X-ray spectroscopy EDS results for GO and rGO are displayed in Figure 2 for comparison. They indicate the distribution of the principal elements and once more attest to the presence of carbon and oxygen in the final sample. Carbon

content in GO and rGO is 74.33% and 86.53%, respectively, whereas oxygen content is 22.51% and 8.56%.
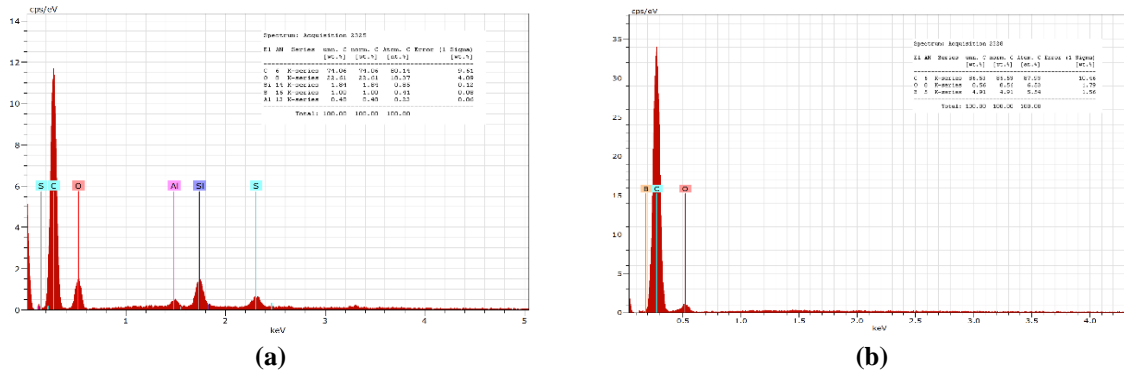

Figure 2. (a) EDS image of GO; **(b)** EDS image of rGO.

The Fourier transform infrared (FTIR) spectra of GO and rGO are depicted in Figure 3. The C and O bond's alkoxy and epoxy vibrations are represented by peaks at locations 1095 cm^{-1} and 1116 cm^{-1}, respectively [11,14]. Peaks at locations 1614 cm^{-1} and 1618 cm^{-1} are associated with the C and C bond's skeletal vibration in unoxidized graphene [13-16]. The hydroxyl group is represented by the peak at positions 2345 cm^{-1} and 2347 cm^{-1} [17,18]. Additionally, the peaks at locations 3435 cm^{-1} and 3443 cm^{-1} are associated with the stretching vibrations of N and H [19].
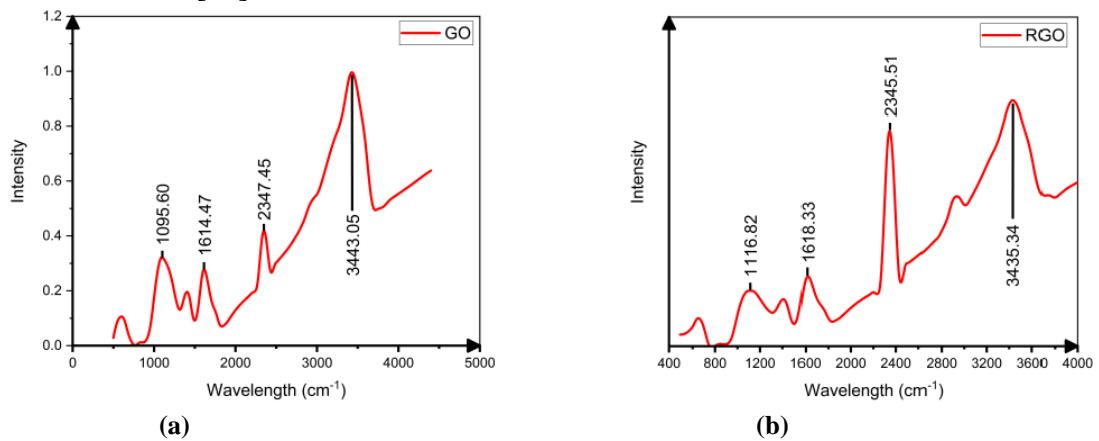
Figure 3. (a) FTIR Spectra of GO; **(b)** FTIR Spectra of rGO.
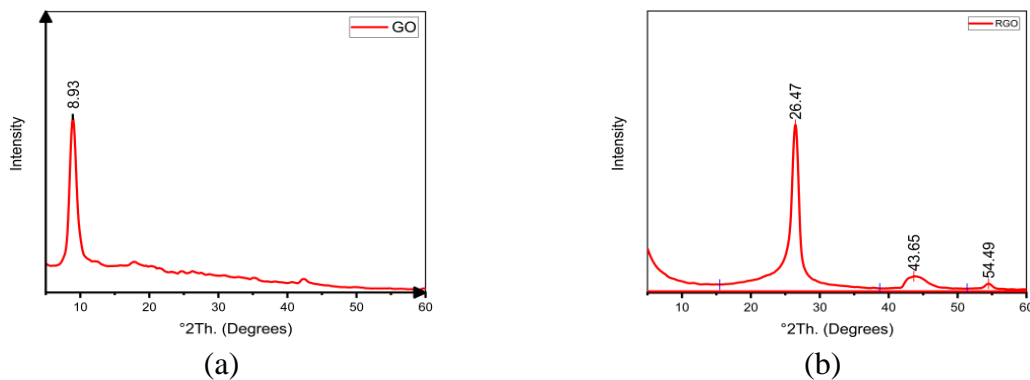
Figure 4. (a) XRD of GO; **(b)** XRD of rGO.

We conducted an X-ray diffraction (XRD) analysis, as depicted in Figure 4, to define GO and rGO morphology further. The peak at 8.93° (002 planes) vanished after GO was oxidized, and a new peak at 26.47° (001 planes) was produced [20]. A bigger angle value strengthens the removal of oxygen from the layers because it reflects a reduction in the distance between the layers.

In order to characterize the structural transformation of graphite into GO and RGO, RAMAN Spectroscopy is a very potent instrument. The two primary characteristics of the Raman spectra are the G band (1352.37 cm^{-1} and 1336.38 cm^{-1}), which represents the retention of the graphite structure, and the D band (1594.21 cm^{-1} and 1565.96 cm^{-1}) which denotes a defect in the graphene structure, as illustrated in Figure 5. The graphene network has effectively preserved the structure, as evidenced by the intensity ratios of the structural defect and graphene network being ID/IG = 0.93 and ID/IG = 0.41 [21].
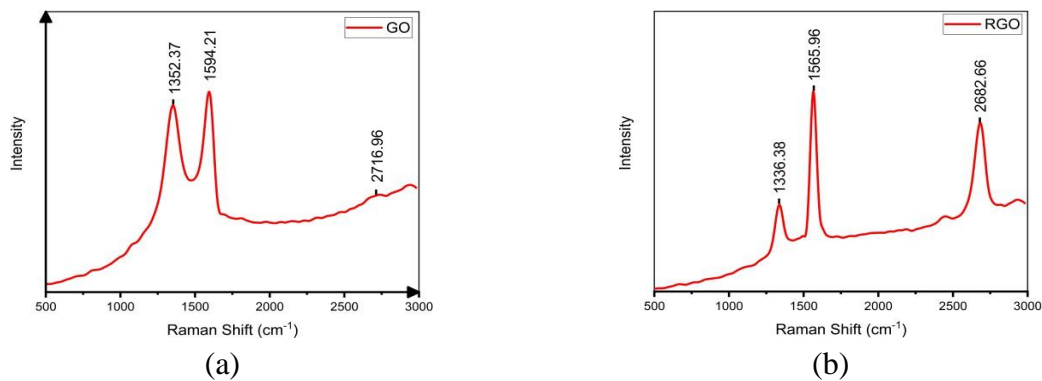
Figure 5. (a) RAMAN Spectra of GO; **(b)** RAMAN Spectra of rGO.

3.2. Colloidal stability analysis.

The GO and rGO nanosuspension with Ethylene Glycol was prepared through extensive ultrasonication. Since the GO peak in Ultraviolet-visible spectroscopy (UV-is) is evident at 238 nm and the UV cut-off wavelength for the Ethylene Glycol is 268 nm [22], there is no GO peak visible in the UV spectra of the GO-EG nanosuspension depicted in Figure 6(a) [23]. Figure 6(b) shows the shoulder of the peak beginning at 270 nm in the case of rGO-EG nanosuspension. This might be interpreted as rGO being present in the nanosuspension -[24].

(DLS) Dynamic light scattering investigations in Figure 7 can be successfully used to determine the size of GO and rGO particles in the GO-EG and rGO-EG nanosuspension. This research aids in determining the size of the particle in the nanosuspension, which is found to be between 111 and 118 nm for rGO and 132 to 151 nm for GO [25,26].
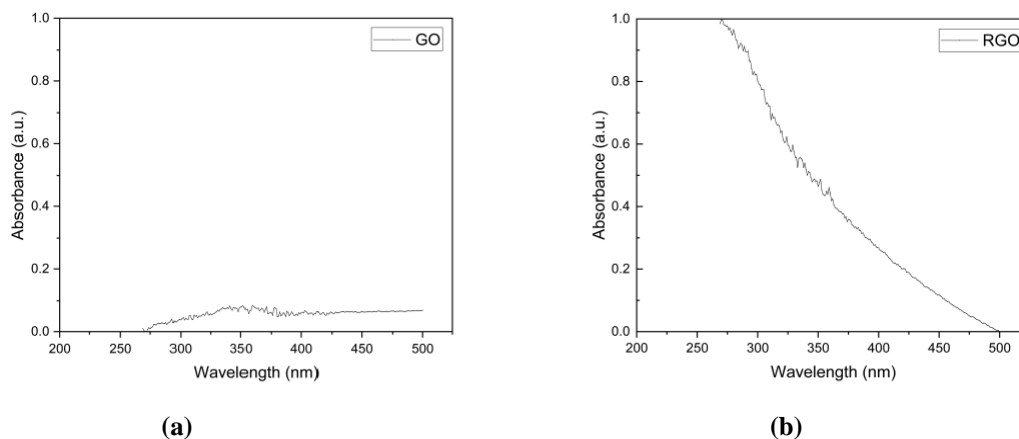

(a) **(b)**

Figure 6. (a) UV-Vis Spectra of GO; **(b)** UV-Vis Spectra of GO.

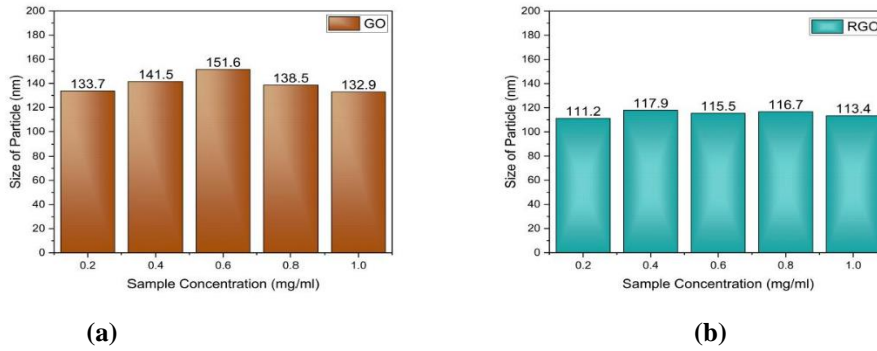|	
(a)	**(b)**

Figure 7. (a) DLS of GO; **(b)** DLS of rGO.

3.3. Thermoacoustic analysis.

The following parameters were measured in the study:

3.3.1. Ultrasonic velocity.

Figure 8, Ultrasonic velocity is among the most significant aspects in assessing the interaction between the molecules and particles in the synthesized nanosuspension. A synthesized sample of GO-EG and rGO-EG have respective ultrasonic velocities examined at 299K, 304K, 309K, and 314K. Values of pure EG were verified with literature, and observation readings were repeated to avoid any experimental inaccuracies [27]. As demonstrated in Figure 8, the variation of ultrasonic velocity with temperature and particle nanofluid gives us information regarding intramolecular and intermolecular interaction. Ultrasonic velocity dips later as we increase the concentration of particles while increasing at pure EG. As the temperature of the other system rises from 299 to 314K, the interaction between GO and EG, rGO, and EG leads to a decrease in ultrasonic velocity. Ultrasonic velocity slows down as the concentration level increases because of a decrease in Brownian motion. GO and EG, rGO, and EG have greater interaction than GO and GO, rGO, and rGO because a rise in temperature leads to a drop in velocity even more than pure EG. Nanosuspension is likely to behave analogously to non-aqueous fluids because as the temperature increases, there is a drop in ultrasonic velocity. That's because as there is a rise in the temperature of the suspension, the molecule moves faster on average and spends less time in the near vicinity. Consequently, the cohesive force and intermolecular adhesive force drop as the temperature increases, leading to enhancing compressibility and lessening of ultrasonic velocity.
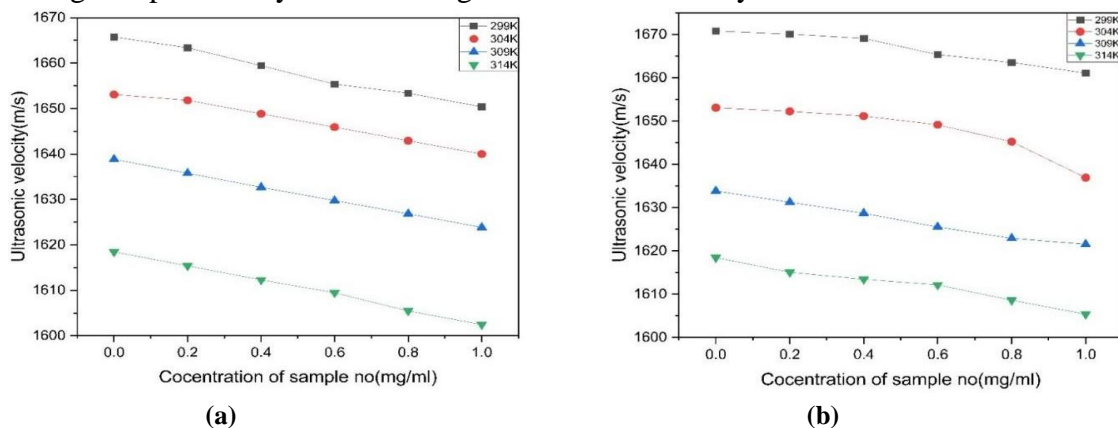

(a)	**(b)**

Figure 8. (a) Velocity in GO-DMF; **(b)** Velocity in rGO-DMF.

3.3.2. Density.

Figure 9. demonstrates that pure EG GO-EG and rGO-EG nanoparticles rise. A slight drop in density is identified. It is well-established that fluid density reduces with rising temperature, so a drop in the density of nanosuspension is consistent with fluid behavior [17]. There is a rise in the density with concentration. The rise of intermolecular interaction leads to a decline in density as the concentration level of the particle increases [28,29].
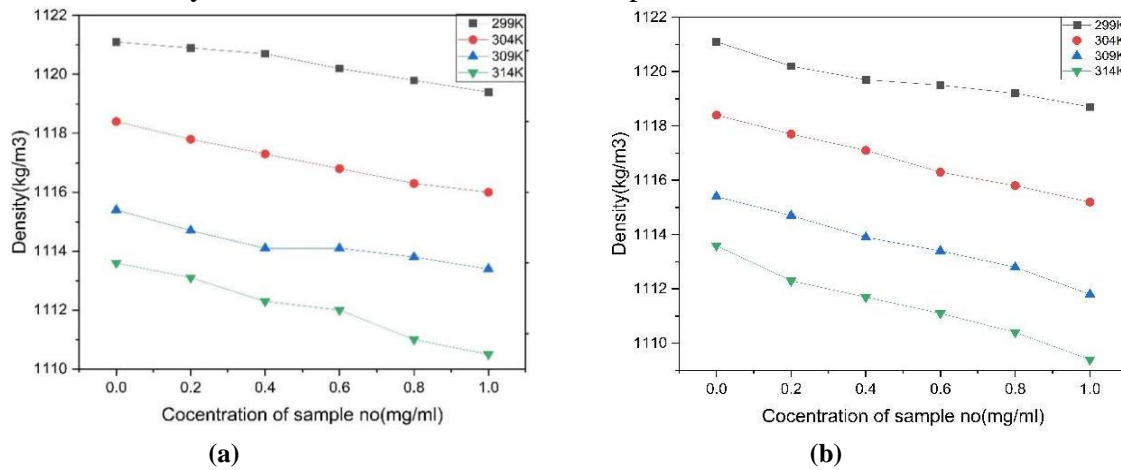

Figure 9. (a) Density in GO-DMF; **(b)** Density in rGO-DMF.

3.3.3. Viscosity.

In Figure 10, the viscosity of GO-EG and rGO-EG considerably increases when GO and rGO nanoparticles are added to a pure EG solution. The interlocking of GO and rGO particles during flow and viscosity increase with increased concentration of nanoparticles [14]. As the temperature viscosity of nanosuspension increases, fluid decreases for both. It's explained by the well-established fact that as the temperature rises, the particle's Brownian motion of nanosuspension increases. Consequently, the nanosuspension's high-temperature flow is higher than the nanosuspension's flow at a lower temperature [30,31].
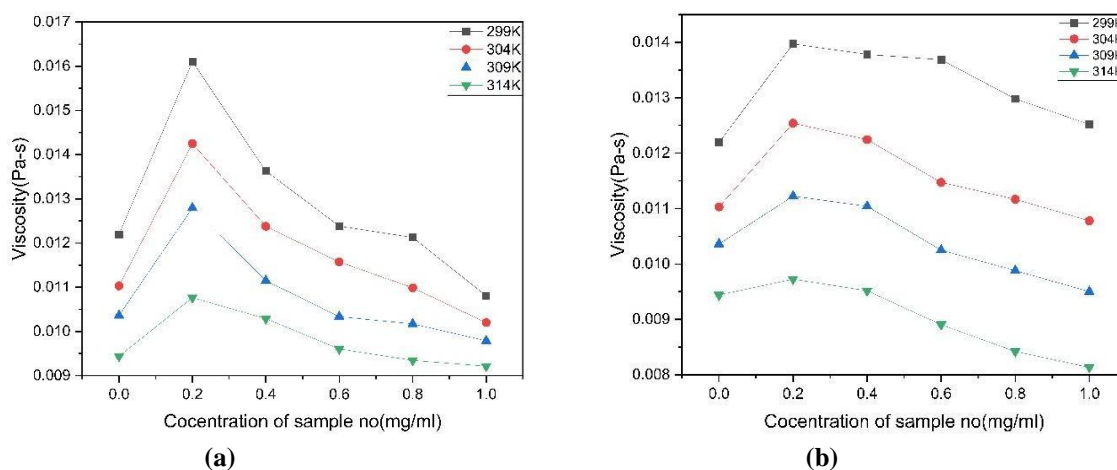

Figure 10. (a) Viscosity in GO-DMF; **(b)** Viscosity in rGO-DMF.

3.3.4. Adiabatic compressibility.

Figure 11, In pure EG, Figure demonstrates how the change in adiabatic compressibility varies when GO and rGO particles were added to the concentration. The

sudden drop that occurs as the nanoparticles are added to the pure EG illustrates the weak fluid interaction. Moreover, the reduction in compressibility signifies that the particles introduced to the based fluid attempted to form complicated structures in the nanosuspension—afterward, both GO-EG and rGO-EG nanosuspension exhibit adiabatic compressibility. There is a reduction in interaction between fluid and particle as the adiabatic compressibility rises, which also presents a complex structure in the system. A rise in adiabatic compressibility with the temperature leads to an increase in the Brownian motion of particles [32].
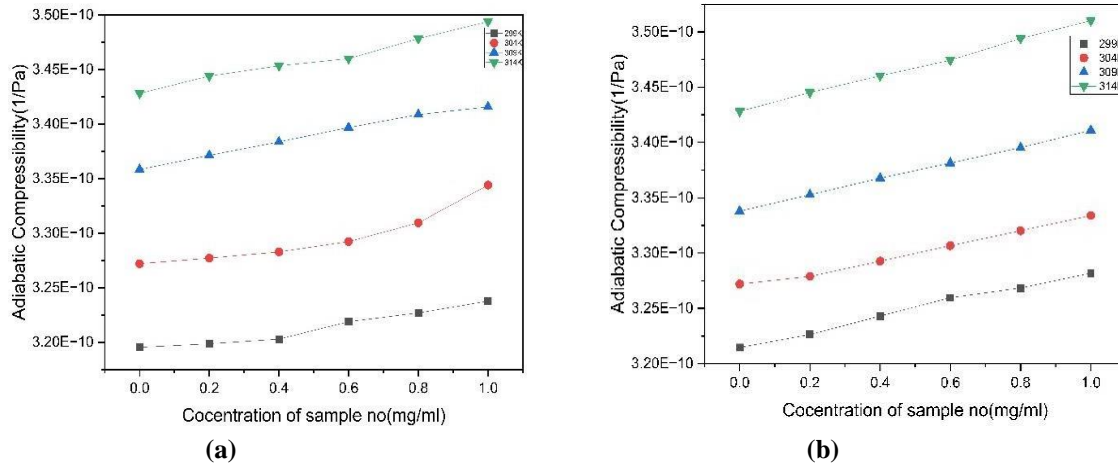

(a)   **(b)**

Figure 11. (a) Compressibility of GO-DMF; **(b)** Compressibility of rGO-DMF.

3.3.5. Acoustic impedance.

Acoustic impedance with particle loading in EG is demonstrated in Figure 12. The rise in acoustical impedance confirmation of interaction among particles in GO-EG and rGO-EG nanosuspension and solute. As concentration increases, there is a reduction in interaction because the particle-fluid interaction is weaker than the particle-particle interaction. Acoustical impedance reduces as fluid's Brownian motion increases with rising temperature. A low concentration leads to a rise in the intermolecular gap, as a rise in the particle fluid concentration offers opposition to the transmission of ultrasonic waves [33,34].
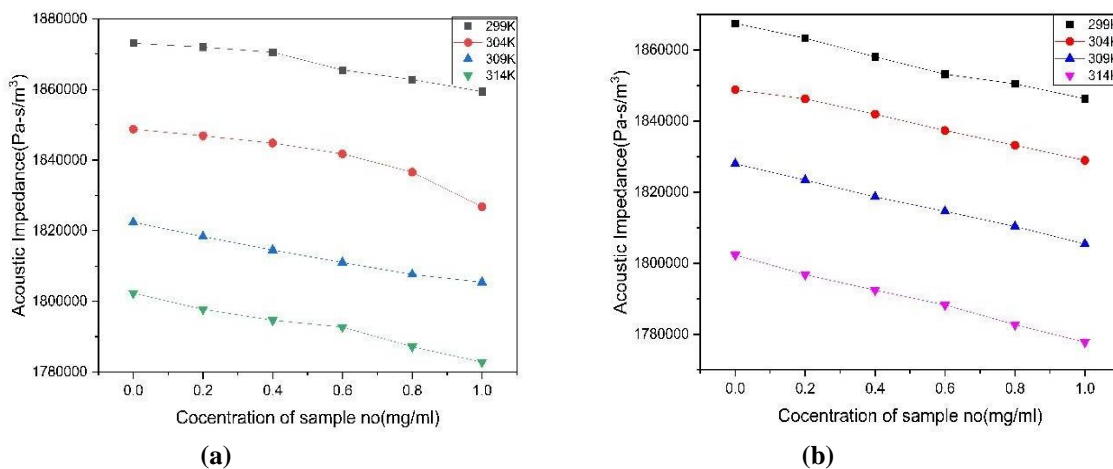

(a)   **(b)**

Figure 12. (a) Acoustical impedance of GO-DMF; **(b)** Acoustical impedance of rGO-DMF.

3.3.6. Ultrasonic attenuation.

Figure 13 demonstrates the variation in ultrasonic attenuation and concentration of nanoparticles in the nanosuspension of GO-EG and rGO-EG. Ultrasonic attenuation rises as the nanoparticles GO and rGO are added to pure EG. GO and rGO interlocking during flow leads to a further rise in ultrasonic attenuation of nanosuspension of GO-EG and rGO-EG. The resistance is established due to the interlocking of GO and rGO, which prevents ultrasonic wave passage from one end to another. The temperature rise also leads to a rise in ultrasonic attenuation.
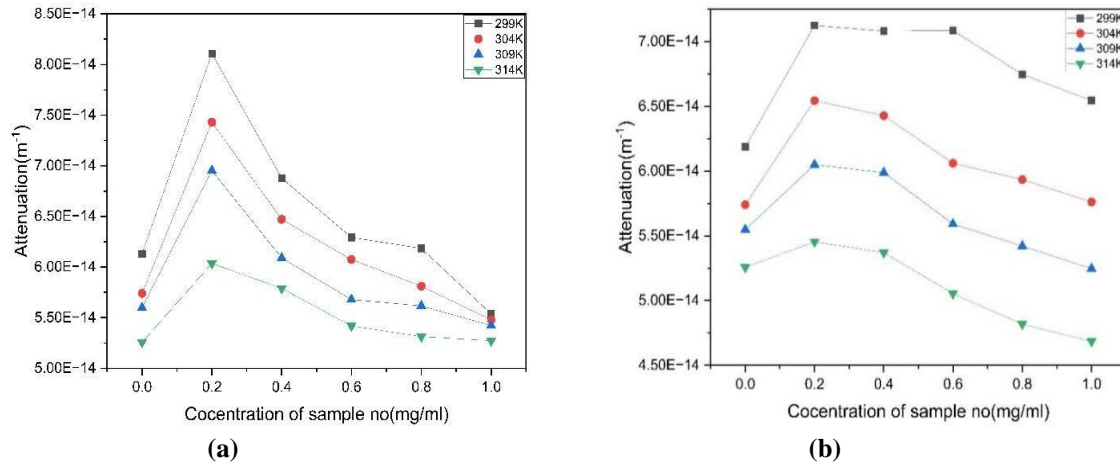

(a)   (b)

Figure 13. (a) Acoustical attenuation of GO-DMF; **(b)** Acoustical attenuation of rGO-DMF.

3.3.7. Bulk modulus.

Figure 14 demonstrates that the nanoparticles of GO and rGO were added to the pure EG nanosuspension, leading to the rise in bulk modulus. Further, with the rise in the level of concentration of GO and rGO to pure EG, the bulk modulus reduces with the rise in temperature [35].
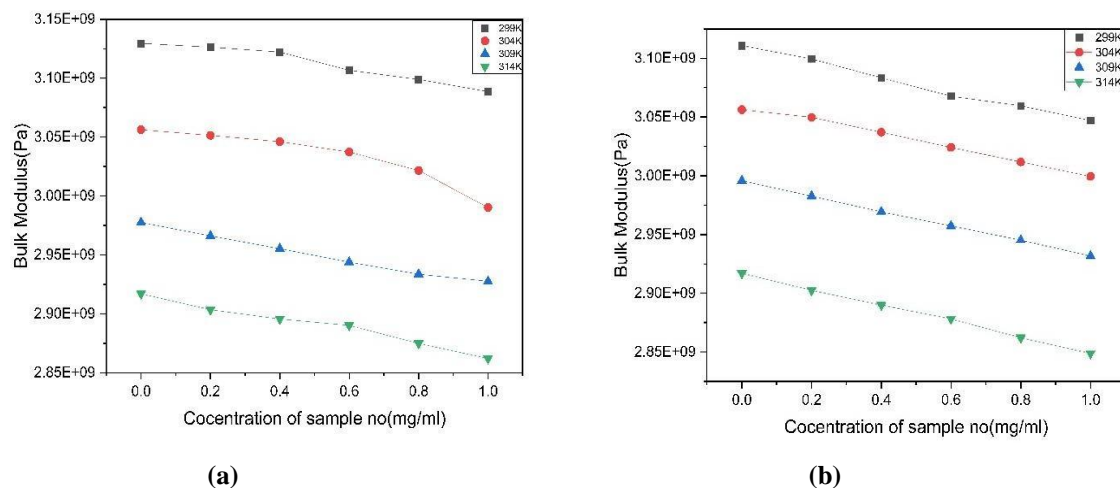

(a)   (b)

Figure 14. (a) Bulk modulus of GO-DMF; **(b)** Bulk modulus of rGO-DMF.

3.3.8. Relaxation time.

Figure 15 demonstrates the relationship between relaxation time and nanoparticle concentration in pure EG. As the GO and rGO nanoparticles have been added to pure EG, there is a sharp rise in relaxation time. Further nanosuspension shows mall variation in relaxation

time. Temperature-dependent relaxation time is influenced by the Brownian motion nanosuspension that grows as the temperature rises [36].
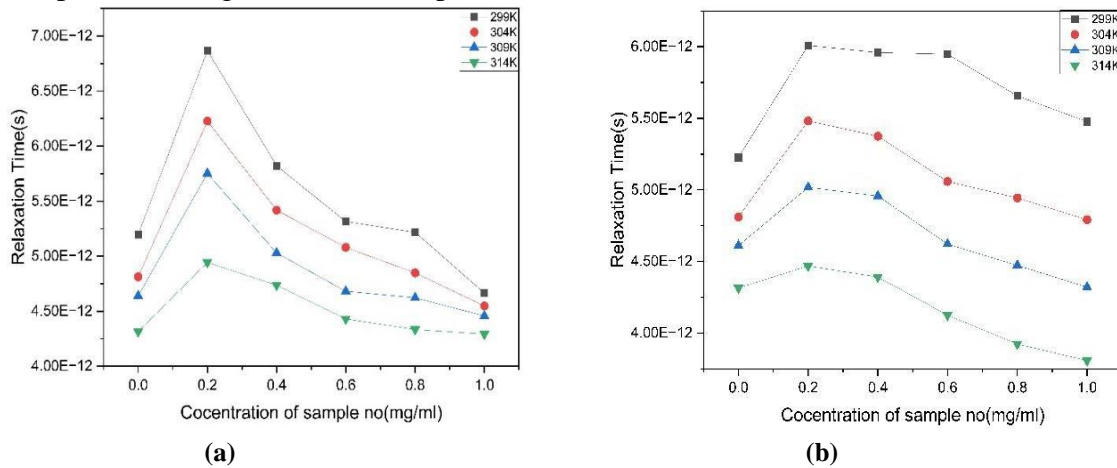

(a)   (b)

Figure 15. (a) Relaxation time of GO-DMF; **(b)** Relaxation time of rGO-DMF.

3.3.8. Intermolecular free length.

Figure 16 demonstrates the variation of intermolecular free length variation with the concentration of nanoparticles in pure EG. As temperature increases, there is a rise in intermolecular free length, which weakens the particle interaction force. It increases as nanoparticles GO and rGO are added to pure EG. The well-established fact is that the decline in fluid-particle interaction contributes to a rise in intermolecular free length [37].
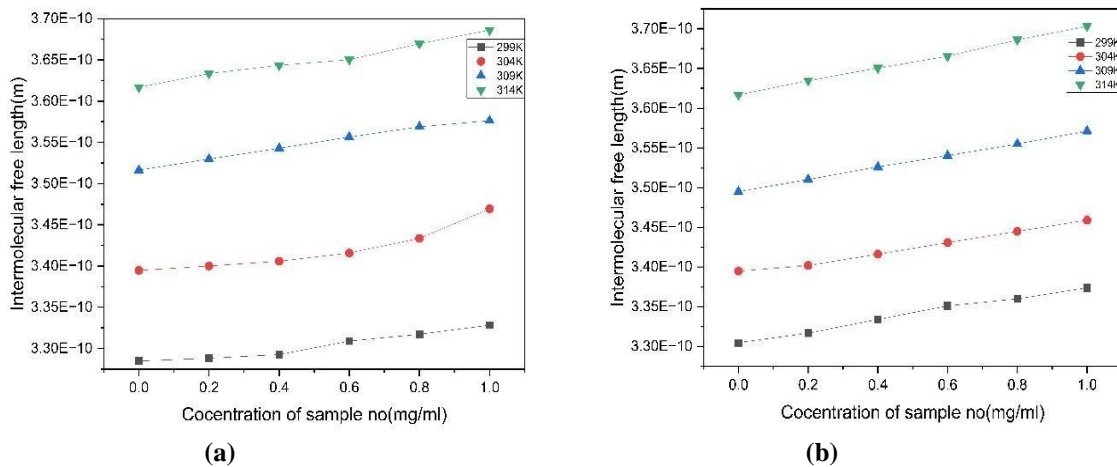

(a)   (b)

Figure 16. (a) Intermolecular free length of GO-DMF; **(b)** Intermolecular free length of rGO-DMF.

4. Conclusion

In this research, Original Hummer's Method was used to synthesize graphene oxide, and then hydrazine monohydrate was used to reduce it. Synthesizing of GO and rGO was verified using numerous methodologies such as FESEM and FTIR. EDS, RAMAN, and XRD verified reduced graphene oxide. Ultrasonication methodology was used to synthesize nanosuspension of GO-EG and rGO-EG ranging at different concentrations. DLS and UV-Vis techniques were employed to demonstrate the stability of nanosuspension. As per acoustical analysis, particle-particles predominate at greater concentrations while fluid predominates at lower concentrations, and rGO-EG and GO-EG show identical behavior.

Funding

This research received no external funding.

Acknowledgments

Presented in 4th International Conference on "Recent Advances in Fundamental and Applied Sciences" (RAFAS-2023)" on March 24-25, 2023, Organized by the School of Chemical Engineering and Physical Sciences, Lovely Professional University, Punjab, India.

Conflicts of Interest

The funders had no role in the study's design; in the collection, analyses, or interpretation of data; in the writing of the manuscript, or in the decision to publish the results.

References

1. Esfahani, M.R.; Languri, E.M.; Nunna, M.R. Effect of particle size and viscosity on thermal conductivity enhancement of graphene oxide nanofluid. *Int. Commun. Heat Mass Transf.* **2016**, *76*, 308-315, https://doi.org/10.1016/j.icheatmasstransfer.2016.06.006.
2. Ou, L.; Song, B.; Liang, H.; Liu, J.; Feng, X.; Deng, B.; Sun, T.; Shao, L. Toxicity of graphene-family nanoparticles: a general review of the origins and mechanisms. *Part. Fibre Toxicol.* **2016**, *13*, 57, https://doi.org/10.1186/s12989-016-0168-y.
3. Alqaed, S.; Mustafa, J.; Sharifpur, M.; Alharthi, M.A. Numerical simulation and artificial neural network modeling of exergy and energy of parabolic trough solar collectors equipped with innovative turbulators containing hybrid nanofluids. *J. Therm. Anal. Calorim.* **2023**, *148*, 8611-8626, https://doi.org/10.1007/s10973-022-11538-7.
4. Nabeel Rashin, M.; Hemalatha, J. Ultrasonics -An Effective Non-invasive Tool to Characterize Nanofluids. In Modeling, Methodologies and Tools for Molecular and Nano-scale Communications. Modeling and Optimization in Science and Technologies; Suzuki, J., Nakano, T., Moore, M., Eds.; Cham, **2017**; Volume 9, 379-399, https://doi.org/10.1007/978-3-319-50688-3_16.
5. Jiříčková, A.; Jankovský, O.; Sofer, Z.; Sedmidubský, D. Synthesis and Applications of Graphene Oxide. *Materials* **2022**, *15*, 920, https://doi.org/10.3390/ma15030920.
6. Xiao, W.; Yu, J.; Xin, J.; Jin, R. Theoretical study on the effect of spacer groups on the nonlinear optical properties of polyvinyl carbazole molecular fragments. *Struct. Chem.* **2020**, *31*, 1471-1479, https://doi.org/10.1007/s11224-020-01504-0.
7. Wang, L.; Huang, Y.; Huang, H. N-doped graphene@polyaniline nanorod arrays hierarchical structures: Synthesis and enhanced electromagnetic absorption properties. *Mater. Lett.* **2014**, *124*, 89-92, https://doi.org/10.1016/j.matlet.2014.03.066.
8. Leena, M.; Srinivasan, S.; Prabhaharan, M. Evaluation of acoustical parameters and thermal conductivity of TiO$_2$-ethylene glycol nanofluid using ultrasonic velocity measurements. *Nanotechnol. Rev.* **2015**, *4*, 449-456, https://doi.org/10.1515/ntrev-2015-0016.
9. Khetib, Y.; Alahmadi, A.; Alzaed, A.; Sharifpur, M.; Cheraghian, G.; Siakachoma, C. Simulation of a parabolic trough solar collector containing hybrid nanofluid and equipped with compound turbulator to evaluate exergy efficacy and thermal-hydraulic performance. *Energy Sci. Eng.* **2022**, *10*, 4304-4317, https://doi.org/10.1002/ese3.975.
10. Wang, Y.; Wu, X.; Zhang, W.; Li, J.; Luo, C.; Wang, Q. Fabrication and enhanced electromagnetic wave absorption properties of sandwich-like graphene@NiO@PANI decorated with Ag particles. *Synth. Met.* **2017**, *229*, 82-88, https://doi.org/10.1016/j.synthmet.2017.05.007.
11. Selvam, C.; Mohan Lal, D.; Harish, S. Thermal conductivity and specific heat capacity of water–ethylene glycol mixture-based nanofluids with graphene nanoplatelets. *J. Therm. Anal. Calorim.* **2017**, *129*, 947-955, https://doi.org/10.1007/s10973-017-6276-6.
12. Zhang, J.; Gao, J.; Song, Q.; Guo, Z.; Chen, A.; Chen, G.; Zhou, S. N-substituted Carboxyl Polyaniline Covalent Grafting Reduced Graphene Oxide Nanocomposites and Its Application in Supercapacitor.

Electrochim. Acta **2016**, *199*, 70-79, https://doi.org/10.1016/j.electacta.2016.03.003.

13. Malik, P.; Kumar, S.; Khushboo; Upmanyu, A.; Kumar, P.; Malik, P. Thermo-acoustical studies of zinc oxide nano particles dispersed nematic liquid crystals mixtures in the temperatures range 283.15 K318.15K. *Liq. Cryst.* **2022**, *49*, 1604-1611, https://doi.org/10.1080/02678292.2022.2102684.

14. Gao, S.; An, Q.; Xiao, Z.; Zhai, S.; Yang, D. Controllable N-Doped Carbonaceous Composites with Highly Dispersed Ni Nanoparticles for Excellent Microwave Absorption. *ACS Appl. Nano Mater.* **2018**, *1*, 5895-5906, https://doi.org/10.1021/acsanm.8b01556.

15. Chen, F.; Yang, Z.; Chen, Z.; Hu, J.; Chen, C.; Cai, J. Density, viscosity, speed of sound, excess property and bulk modulus of binary mixtures of γ-butyrolactone with acetonitrile, dimethyl carbonate, and tetrahydrofuran at temperatures (293.15 to 333.15) K. *J. Mol. Liq.* **2015**, *209*, 683-692, https://doi.org/10.1016/j.molliq.2015.06.041.

16. Sheshmani, S.; Ashori, A.; Fashapoyeh, M.A. Wood plastic composite using graphene nanoplatelets. *Int. J. Biol. Macromol.* **2013**, *58*, 1-6, https://doi.org/10.1016/j.ijbiomac.2013.03.047.

17. Muzyka, R.; Kwoka, M.; Smędowski, Ł.; Díez, N.; Gryglewicz, G. Oxidation of graphite by different modified Hummers method. *New Carbon Mater.* **2017**, *32*, 15-20, https://doi.org/10.1016/S1872-5805(17)60102-1.

18. Ma, J.; Liu, J.; Zhu, W.; Qin, W. Solubility study on the surfactants functionalized reduced graphene oxide. *Colloids Surf. A: Physicochem. Eng. Asp.* **2018**, *538*, 79-85, https://doi.org/10.1016/j.colsurfa.2017.10.071.

19. Pereira, J.E.; Moita, A.S.; Moreira, A.L.N. The pressing need for green nanofluids: A review. *J. Environ. Chem. Eng.* **2022**, *10*, 107940, https://doi.org/10.1016/j.jece.2022.107940.

20. Luo, J.; Xu, Y.; Yao, W.; Jiang, C.; Xu, J. Synthesis and microwave absorption properties of reduced graphene oxide-magnetic porous nanospheres-polyaniline composites. *Compos. Sci. Technol.* **2015**, *117*, 315-321, https://doi.org/10.1016/j.compscitech.2015.07.008.

21. Vinod, S.; Philip, J. Thermal and rheological properties of magnetic nanofluids: Recent advances and future directions. *Adv. Colloid Interface Sci.* **2022**, *307*, 102729, https://doi.org/10.1016/j.cis.2022.102729.

22. Katzmarek, D.A.; Mancini, A.; Maier, S.A.; Iacopi, F. Direct synthesis of nanopatterned epitaxial graphene on silicon carbide. *Nanotechnology* **2023**, *34*, 405302, https://doi.org/10.1088/1361-6528/ace369.

23. Kumar, L.H.; Kazi, S.N.; Masjuki, H.H.; Zubir, M.N.M. A review of recent advances in green nanofluids and their application in thermal systems. *J. Chem. Eng.* **2022**, *429*, 132321, https://doi.org/10.1016/j.cej.2021.132321.

24. Rudyak, V. Thermophysical Characteristics of Nanofluids and Transport Process Mechanisms. *J. Nanofluids* **2019**, *8*, 1-16, https://doi.org/10.1166/jon.2019.1561.

25. Shin, H.; Lee, S. Fabrication of suspended graphene field-effect transistors by the sandwich method. *Curr. Appl. Phys.* **2023**, *48*, 42-46, https://doi.org/10.1016/j.cap.2023.01.012.

26. Feng, W.; Wang, Y.; Chen, J.; Wang, L.; Guo, L.; Ouyang, J.; Jia, D.; Zhou, Y. Reduced graphene oxide decorated with in-situ growing ZnO nanocrystals: Facile synthesis and enhanced microwave absorption properties. *Carbon* **2016**, *108*, 52-60, https://doi.org/10.1016/j.carbon.2016.06.084.

27. Zhou, S.; Zhang, H.; Zhao, Q.; Wang, X.; Li, J.; Wang, F. Graphene-wrapped polyaniline nanofibers as electrode materials for organic supercapacitors. *Carbon* **2013**, *52*, 440-450, https://doi.org/10.1016/j.carbon.2012.09.055.

28. Anagnostopoulos, G.; Sygellou, L.; Paterakis, G.; Polyzos, I.; Aggelopoulos, C.A.; Galiotis, C. Enhancing the adhesion of graphene to polymer substrates by controlled defect formation. *Nanotechnology* **2019**, *30*, 015704, https://doi.org/10.1088/1361-6528/aae683.

29. Vărdaru, A.; Huminic, G.; Huminic, A.; Fleacă, C.; Dumitrache, F.; Morjan, I. Aqueous hybrid nanofluids containing silver-reduced graphene oxide for improving thermo-physical properties. *Diam. Relat. Mater.* **2023**, *132*, 109688, https://doi.org/10.1016/j.diamond.2023.109688.

30. Roy, I.; Sarkar, G.; Mondal, S.; Rana, D.; Bhattacharyya, A.; Saha, N.R.; Adhikari, A.; Khastgir, D.; Chattopadhyay, S.; Chattopadhyay, D. Synthesis and characterization of graphene from waste dry cell battery for electronic applications. *RSC Adv.* **2016**, *6*, 10557-10564, https://doi.org/10.1039/C5RA21112C.

31. Nabeel Rashin, M.; Hemalatha, J. A novel ultrasonic approach to determine thermal conductivity in CuO–ethylene glycol nanofluids. *J. Mol. Liq.* **2014**, *197*, 257-262, https://doi.org/10.1016/j.molliq.2014.05.024.

32. Anju; Yadav, R.S.; Pötschke, P.; Pionteck, J.; Krause, B.; Kuřitka, I.; Vilčáková, J.; Škoda, D.; Urbánek, P.; Machovský, M.; Masař, M.; Urbánek, M. $Cu_xCo_{1-x}Fe_2O_4$ (x= 0.33, 0.67, 1) Spinel Ferrite Nanoparticles Based Thermoplastic Polyurethane Nanocomposites with Reduced Graphene Oxide for Highly Efficient Electromagnetic Interference Shielding. *Int. J. Mol. Sci.* **2022**, *23*, 2610,

https://doi.org/10.3390/ijms23052610.

33. Nanda, A.; Tiadi, A.; Mallik, S.K.; Giri, R.; Nath, G. Ultrasonic Characterization of Silver Nano Fluid. *IOP Conf. Ser.: Mater. Sci. Eng.* **2018**, *360*, 012064, https://doi.org/10.1088/1757-899X/360/1/012064.

34. Smaisim, G.F.; Abed, A.M.; Al-Madhhachi, H.; Hadrawi, S.K.; Al-Khateeb, H.M.M.; Kianfar, E. Graphene-Based Important Carbon Structures and Nanomaterials for Energy Storage Applications as Chemical Capacitors and Supercapacitor Electrodes: a Review. *BioNanoScience* **2023**, *13*, 219-248, https://doi.org/10.1007/s12668-022-01048-z.

35. Kanti, P.; Sharma, K.V.; Khedkar, R.S.; Rehman, T.U. Synthesis, characterization, stability, and thermal properties of graphene oxide based hybrid nanofluids for thermal applications: Experimental approach. *Diam. Relat. Mater.* **2022**, *128*, 109265, https://doi.org/10.1016/j.diamond.2022.109265.

36. Gutiérrez-Cruz, A.; Ruiz-Hernández, A.R.; Vega-Clemente, J.F.; Luna-Gazcón, D.G.; Campos-Delgado, J. A review of top-down and bottom-up synthesis methods for the production of graphene, graphene oxide and reduced graphene oxide. *J. Mater. Sci.* **2022**, *57*, 14543-14578, https://doi.org/10.1007/s10853-022-07514-z.

37. Lee, J.; Lee, S.; Cho, C.; Kim, S. Experimental study and modeling of the energy density and time-dependent rheological behavior of carbon nanotube nanofluids with sonication. *Int. J. Heat Mass Transf.* **2022**, *192*, 122941, https://doi.org/10.1016/j.ijheatmasstransfer.2022.122941.